

1 **A +CG flash caused by a sequence of bidirectional leaders that served to form a**
2 **ground-reaching branch of a pre-existing horizontal channel**

3 Bin Wu^{1,2}, Weitao Lyu^{1,2}, Qi Qi^{1,2}, Ying Ma^{1,2}, Lyuwen Chen³, Ruijiao Jiang^{1,2,5}, Yanan Zhu⁴
4 and Vladimir A. Rakov⁵

5 ¹State Key Laboratory of Severe Weather, Chinese Academy of Meteorological Sciences,
6 Beijing 100081, China

7 ²Laboratory of Lightning Physics and Protection Engineering, Chinese Academy of
8 Meteorological Sciences, Beijing 100081, China

9 ³Institute of Tropical and Marine Meteorology, China Meteorological Administration,
10 Guangzhou 510080, China

11 ⁴Earth System Science Center, University of Alabama in Huntsville, Huntsville, Alabama,
12 USA

13 ⁵Department of Electrical and Computer Engineering, University of Florida, Gainesville,
14 Florida, USA

15 **Corresponding author:** Weitao Lyu (lyuwt@foxmail.com)

16
17 **Key Points:**

- 18 • Bidirectional leaders developed below a previously formed horizontal channel and
19 served to form a new positive branch that attached to the ground
- 20 • Connection of the negative (upper) end of each bidirectional leader to the horizontal
21 channel resulted in abrupt elongation of the positive (lower) end
- 22 • Numerous negative streamer-like filaments extended sideways from the horizontal
23 channel in response to the injection of negative charge associated with the +CG

24 **Abstract**

25 High-speed video and electric field change data were used to analyze the initiation and
26 propagation of four predominantly vertical bidirectional leaders making connection to a
27 predominantly horizontal channel previously formed aloft. The four bidirectional leaders
28 sequentially developed along the same path and served to form a positive branch of the
29 horizontal in-cloud channel, which became a downward positive leader producing a 135-kA
30 positive cloud-to-ground (+CG) return stroke. The positive (lower) end of each bidirectional
31 leader elongated abruptly at the time of connection of the negative (upper) end to the
32 pre-existing channel aloft. Twenty-six negative streamer-like filaments (resembling recently
33 reported “needles”) extended sideways over ~100 to 750 m from the pre-existing horizontal
34 channel at speeds of ~ 0.5 to 1.9×10^7 m/s, in response to the injection of negative charge
35 associated with the +CG.

36 **Plain Language Summary**

37 This paper presents high-speed video records that show for the first time how a sequence of
38 predominantly vertical bidirectional leaders can lead to formation of a positive branch of the
39 previously formed predominantly horizontal channel aloft, with this branch eventually making
40 contact with the ground and initiating a positive cloud-to-ground (+CG) return stroke.
41 Observations were performed at the Tall-Object Lightning Observatory in Guangzhou
42 (TOLOG), China. This study helps to improve our understanding of one of the initiation
43 mechanisms of +CG flashes that involves downward branching of in-cloud lightning channels.

44 **1. Introduction**

45 One of the most challenging issues in the physics of lightning is the interpretation of the
46 initiation mechanisms of positive cloud-to-ground (+CG) discharges. According to Rakov and
47 Uman (2003), downward positive lightning can be produced by a cloud discharge, or initiated
48 by a branch of a cloud discharge. Recently, Nag and Rakov (2012) described 6 conceptual
49 cloud charge configurations and scenarios that were observed or hypothesized to give rise to
50 positive lightning, with one of scenarios being a positive branch of an in-cloud discharge
51 channel (see Section 2.6 and Figure 1f in their paper). High-speed video images of such flashes

52 are found in the works of Kong et al. (2008) and Saba et al. (2009). However, so far there are no
53 documented cases showing the process of such branch formation. Observations show that
54 branches of in-cloud channels can involve a sequence of bidirectional leaders (Warner et al.,
55 2016; Yuan et al., 2019) that, in effect, facilitate connection of a channel aloft to ground (Tran
56 and Rakov 2016).

57 High-speed video and VHF observations are two widely used methods to analyze the
58 dynamics of leader initiation and propagation. However, the relatively strong negative
59 breakdown VHF signals associated with the negative end of bidirectional leaders, tend to mask
60 the relatively weak positive breakdown VHF signals associated with the simultaneously
61 propagating positive end (Shao et al., 1999). Consequently, it is often difficult for VHF
62 imaging systems to detect the positive end of bidirectional leaders. Bidirectional propagation
63 of leaders can be detected (imaged) with high-speed video cameras that have yielded important
64 results published by Jiang et al. (2014), Montanyà et al. (2015), Kaneyoshi et al. (2015),
65 Kostinskiy et al. (2015), Warner et al. (2016), Tran and Rakov (2016), Yuan et al. (2019), and
66 Wu et al. (2019a). In particular, Montanyà et al. (2015) reported a recording of bidirectional
67 intracloud lightning (IC) initiation in virgin air at ~11,000 frames per second (fps). Tran and
68 Rakov (2016) observed that the negative end of a bidirectional leader contacted ground and
69 produce a negative cloud-to-ground (-CG) return stroke. However, bidirectional leaders often
70 develop completely inside the cloud, which makes their optical imaging difficult. Only a few
71 quality recordings are presently available. As a result, the details of dynamics of bidirectional
72 leaders resulting in the formation of a ground-reaching leader are still not completely
73 understood.

74 Positive lightning discharges account for about 10% of all CG discharges (e.g., Rakov,
75 2003), so positive lightning discharges are considerably less studied and understood than their
76 negative counterparts. Furthermore, most of the existing optical observations of +CG flashes
77 can only yield some characteristics after the leader emerges from the cloud. To the best of our
78 knowledge, to date, there are no optical records of the complete dynamics of +CG flashes.
79 High-speed video observations reviewed above confirm that in-cloud channels giving rise to

80 CG discharges can be produced by bidirectional leaders. However, details of the formation of a
81 downward positively charged ground-reaching branch have not been reported before.

82 In this paper, we present optical and electric field observations of the formation process
83 of ground-reaching positive branch of an in-cloud channel initiating a +CG, with this process
84 being documented for the first time. The observations were performed at the Tall-Object
85 Lightning Observatory in Guangzhou (TOLOG), China. The dynamics of all stages of the +CG
86 flash are examined and discussed in detail. Among other things, our records show flickering
87 streamer-like filaments (resembling recently reported “needles”, Hare et al., 2019; Pu and
88 Cummer, 2019) extending sideways from the horizontal in-cloud channel energized by the
89 +CG.

90 **2. Instrumentation and Data**

91 The TOLOG (Lu et al., 2012, 2013; Qi et al., 2019; Wu et al. 2019b) is located on the
92 roof of an approximately 100-m-high building of the Guangdong Meteorological Bureau. The
93 optical instrumentation used in this study consisted of a lightning channel imager (LCI) and
94 two high-speed video cameras (HC-1 and HC-2) operating at different framing rates
95 (20,000-fps and 50,000-fps, respectively). The focal lengths of HC-1 and HC-2 were 14 and 20
96 mm, respectively, and the record lengths were 50 and 20 ms, respectively. The corresponding
97 pre-trigger times were 25, and 10 ms and the corresponding spatial resolutions were 1024
98 pixels \times 1024 pixels and 512 pixels \times 272 pixels. The framing rate and focal length of the
99 lightning channel imager (LCI) were 50-fps and 5 mm, respectively. The record length,
100 corresponding pre-trigger time and corresponding spatial resolution of LCI were 2 s, 500 ms,
101 and 780 pixels \times 582 pixels, respectively.

102 Electric field changes were measured using a set of fast and slow antenna systems. The
103 time constants of the fast and slow antennas were 1 ms and 6 s, respectively, and the sampling
104 rate of the two field measuring systems was 10 MHz. The record lengths and pre-trigger times
105 of the fast and slow antenna systems were 1 s and 100 ms, respectively. The measurement
106 ranges of the fast and slow antenna systems were ± 100 kV/m and ± 200 kV/m, respectively, and
107 the vertical resolution of each of them was 12-bit.

108 Signals from one of the eight channels of the Lightning Attachment Process
109 Observation System (LAPOS, Wang et al., 2011) recorded by a digital oscilloscope was used
110 for triggering the cameras and the field measuring systems. Each trigger event was
111 time-stamped using a GPS clock with accuracy of 30 ns. In addition, we obtained information
112 on the location of lightning channel ground termination point, the time of return stroke, and the
113 estimated peak current of the +CG return stroke from the Guangdong-Hong Kong-Macao
114 Lightning Location System (GHMLLS).

115 The +CG flash (denoted F17149) considered here contained a single stroke. The
116 GHMLLS reported that stroke to be located approximately 17 km from the observation station
117 and estimated its peak current to be approximately +135 kA. In this paper, we analyzed the
118 characteristics of bidirectional leaders involved in the initiation and development of the +CG.
119 Additionally, we examined streamer-like filaments extending sideways from the horizontal
120 in-cloud channel energized by the +CG. All the lengths and speeds presented are two-
121 dimensional (2-D) and estimated based on the distance between the +CG ground termination
122 point and TOLOG. All times are relative to the onset of the return stroke of the +CG flash. The
123 atmospheric electricity electric field sign convention was used in this study.

124 **3. Data Presentation and Results**

125 The LCI operated at 50-fps (20-ms interframe interval) with a recording time of 2
126 second and completely recorded the entire +CG lightning flash (see Movie S1 in the supporting
127 information). Figure 1 shows 7 consecutive LCI images, with an exposure time of
128 approximately 20 ms each, with the time stamp on each image being the end of exposure time
129 relative to the return-stroke onset. No luminous channels were seen for about 500 ms in the LCI
130 record prior to the -79-ms frame. A short floating channel appeared in the -79-ms frame (see
131 the smaller rectangular box and its expansion in Figure 1b). The floating channel became
132 visible during the -99 to -79 ms time interval and then clearly exhibited bidirectional
133 development extending horizontally over about 15 km from -79 to -59 ms (see Figure 1c).

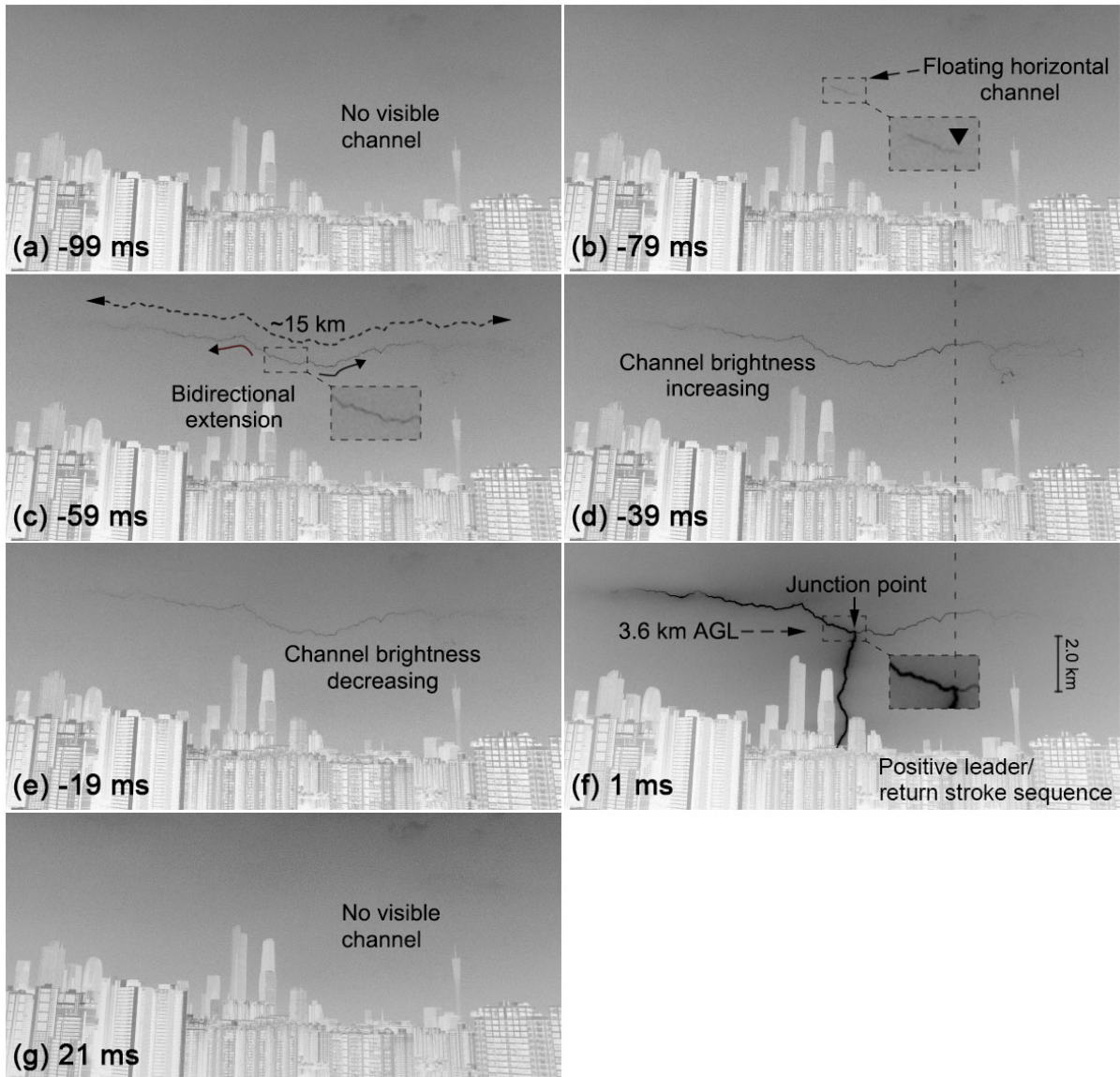
134 In the next two frames (see Figures 1d and 1e), the bidirectional leader channel did not
135 exhibit further extension, but its brightness increased from -59 to -39 ms and then decreased
136 from -39 to -19 ms. The predominantly vertical (positive leader/return stroke sequence)

137 channel connecting the previously formed predominantly horizontal channel with the ground is
138 seen in Figure 1f. However, due to the insufficient temporal resolution of LCI, the dynamics of
139 that connection is not resolved in Figure 1. Note that the junction point between the positive
140 leader/return stroke channel and the previously formed horizontal channel was near the right
141 end of the initial horizontal channel segment seen in Figure 1b (see vertical broken line passing
142 through Figures 1b, 1d, and 1f).

143 We now present our records obtained using the high-speed video camera (HC-1)
144 operating at 20,000-fps (50- μ s interframe interval) with a recording time of 50 ms. These
145 records (see Movie S2 in the supporting information) clearly show that the downward positive
146 leader evolved from a sequence of four bidirectional leaders that developed along the same,
147 predominantly vertical path below the predominantly horizontal channel whose development is
148 seen in Figure 1. Figure 2a shows a composite image of 40 selected HC-1 frames before the
149 onset of the +CG return stroke. These frames were selected to best display the geometry of the
150 horizontal channel aloft and the following four bidirectional leaders, the last of which
151 completed the formation of the downward branch of the horizontal channel, which forged its
152 way to ground and produced the +CG return stroke.

153 Figure 2b shows the image brightness record along with the fast and slow antenna
154 system electric field changes. The initial (preliminary) breakdown type pulses (labeled IBPs) in
155 the fast electric field change record (labeled FA in Figure 2b) that occurred about 60 ms prior to
156 the return stroke (labeled +RS) corresponds to the full (about 15 km) extension of the
157 horizontal channel seen in Figure 1c (-59-ms, end of exposure time). Between -50 and -40 ms,
158 K change type signatures are seen in the fast electric field change record. Note that between -59
159 and -39 ms, the brightness of the horizontal channel increased (see Figure 1d). It follows from
160 Figure 1 that no vertical channel was formed before -19 ms. However, at that time the slow
161 electric field change record, labeled SA in Figure 2, shows significant positive (opposite to the
162 +RS) field deflection, which is indicative of the motion of positive charge toward the observer.
163 In fact, the positive field deflection started at about -60 ms, and the slow field change between
164 -60 ms and 0 is characteristic of downward positive leader signature, although the downward
165 extension apparently did not start until -19 ms or so. It is likely that the positive charge motion

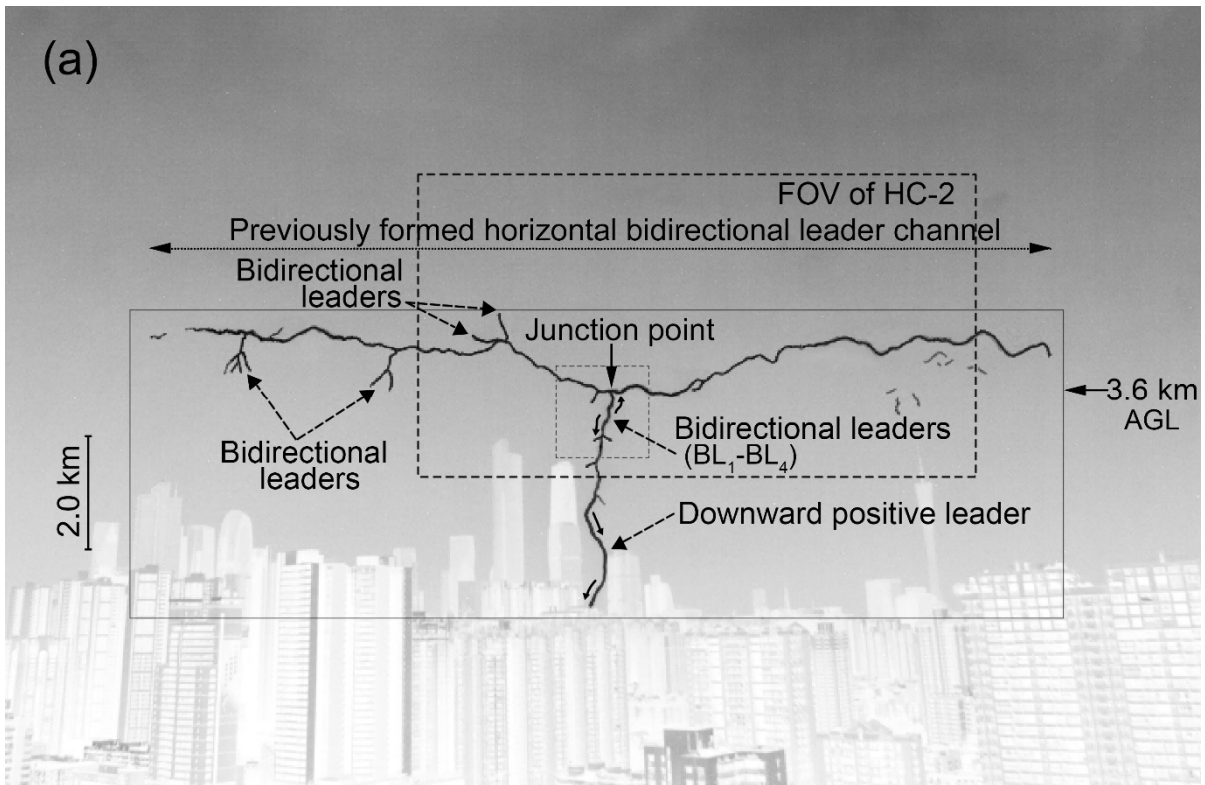
166 toward the observation station between -60 and -19 ms is indicative of the entire horizontal
 167 channel being charged positively. The beginning and intensification of this latter process are
 168 marked by IBPs and K changes, respectively, seen in the FA record in Figure 2b.



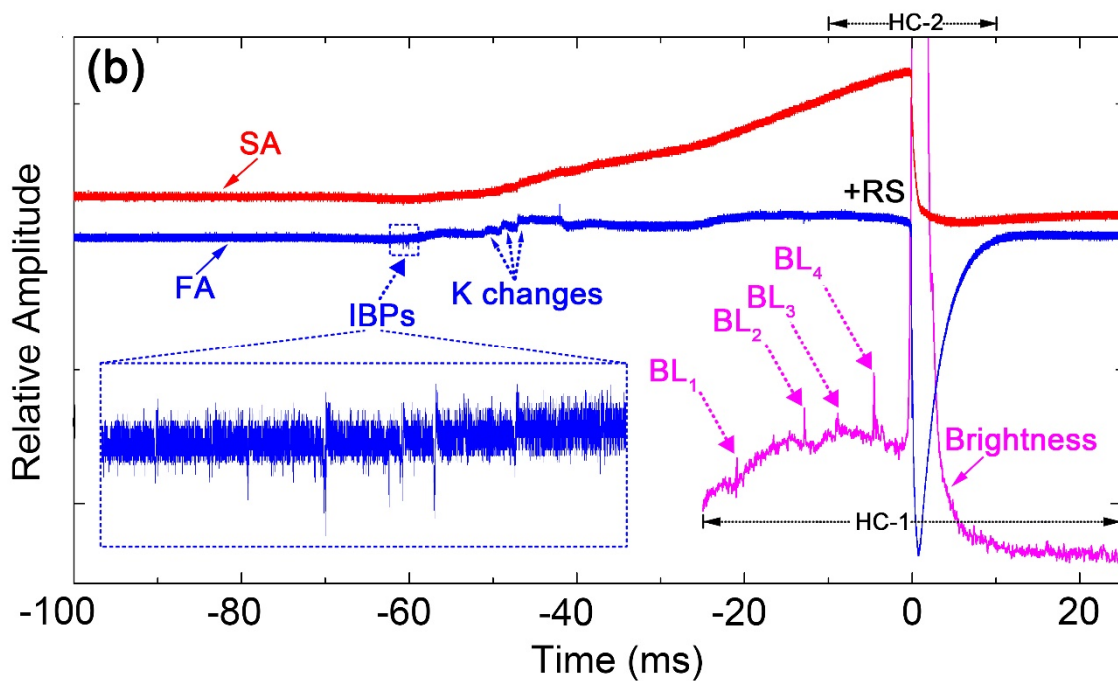
169
 170 **Figure 1.** Seven consecutive images obtained using the lightning channel imager (LCI)
 171 operating at 50 frames per second (20-ms interframe interval). The time stamp on each image
 172 corresponds to the end of exposure time, adjusted based on synchronized images from HC-1.
 173 The images were cropped, inverted, and contrast enhanced. Portions of images in smaller
 174 broken-line boxes are shown enlarged in (b), (c), and (f). Small inverted triangle in (b)
 175 indicates the inferred origination point of the predominantly horizontal channel, whose
 176 development is seen in (b) and (c).

177 Four bidirectional leaders (BL₁-BL₄) associated with formation of downward positive
178 leader occurred approximately 20, 12, 9, and 4 ms before the onset of the +CG return stroke
179 (see the brightness trace in Figure 2b). BL₁ to BL₄ produced no pronounced electric field
180 changes (see the FA and SA traces in Figure 2b), because they were relatively far
181 (approximately 17 km) from observation station. The upper end of each bidirectional leader
182 extended upward (this extension is imaged for BL₁, BL₃, and BL₄ and inferred for BL₂) and
183 contacted the previously formed horizontal channel, forming a downward branch of the
184 horizontal channel that eventually made contact with the ground. The height of the junction
185 point was approximately 3.6 km above ground level (AGL). The polarity of charge transfer to
186 ground was positive, based on the negative electric field change at $t = 0$ (see +RS in Figure 2b).
187 Consequently, the lower end of each bidirectional leader must have been positive, with the
188 upper end being negative and the horizontal channel aloft (at least near the junction point)
189 being positive.

190 During the +CG return stroke stage, the left part of the horizontal channel was much
191 brighter than the right one (see Movies S2 and S3 in the supporting information), which
192 suggests that positive charge was supplied to the vertical channel to ground mostly by the left
193 part of the horizontal channel. However, the brightness of the right part also increased during
194 the return-stroke stage and, hence, it also participated in delivering positive charge to the
195 junction point (in other words, the negative charge injected by the +CG return stroke into the
196 junction point moved both to the left and to the right along the horizontal channel). Further,
197 during BL₁-BL₄ (approximately -20 ms to 0), the electric field was dominated by the motion of
198 positive charge toward the observation station (see the SA trace in Figure 2b), which indicates
199 that the middle part of the floating horizontal channel (near the prospective junction point) was
200 positive. There were other bidirectional leaders that served to form short branches in the left
201 part of the horizontal channel (see Bidirectional leaders appeared on the left part of the
202 horizontal channel in Figure 2a). Those are not further discussed in this paper.



203

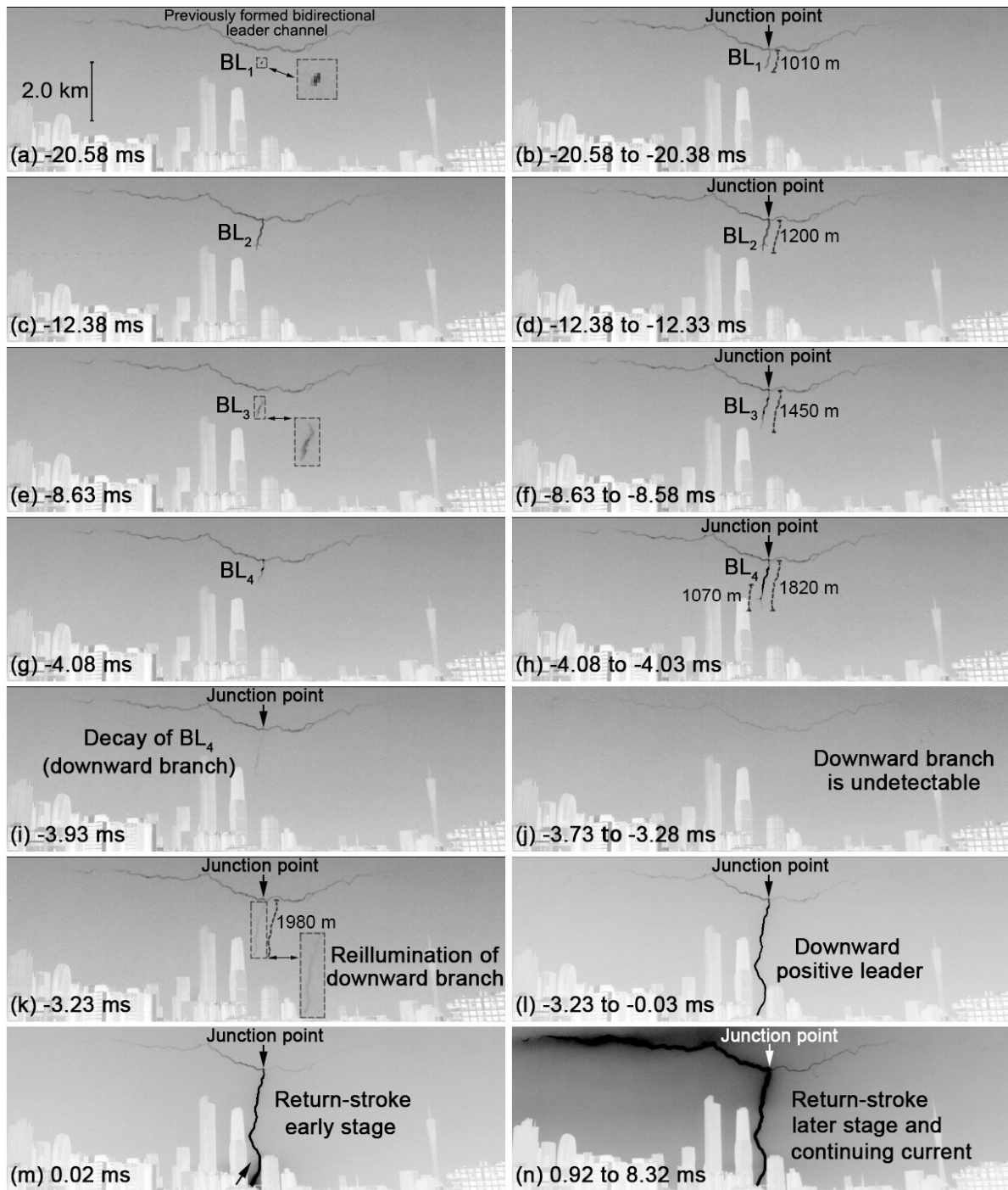


204

205 **Figure 2.** (a) Composite image of 40 selected frames (from -25 to -0.05 ms) obtained using
 206 HC-1 operating at 20,000 frames per second ($50\text{-}\mu\text{s}$ interframe interval), showing the geometry
 207 of downward positive leader channel to ground (formed via a sequence of four bidirectional
 208 leaders, which connected to the previously formed horizontal channel aloft). (b) Synchronized
 209 optical image brightness (the sum of gray values of all pixels in each HC-1 image) within -25 to

210 25 ms time window, and fast (FA) and slow (SA) electric field change records (from -100 to 25
211 ms). The image shown in (a) was cropped, inverted, and contrast enhanced. The curved arrows
212 indicate the observed directions of channel extension. Single-frame and composite HC-1
213 images of the solid-line rectangular area seen in (a) that show the salient features of the
214 discharge development after the formation of the horizontal channel aloft are presented in
215 Figures 2a-2n. The dashed-line rectangular box in (a) shows the field of view (FOV) of HC-2.
216 The time window corresponding to images recorded by HC-2 is from -10 to 10 ms. The larger
217 dashed-line rectangular box in (b) is an expanded view for the smaller dashed-line rectangular
218 box labeled IBPs. Labels BL₁–BL₄ are used to mark four bidirectional leaders examined in
219 detail. AGL = above ground level; +RS = positive return stroke; SA = slow antenna; FA = fast
220 antenna; IBPs = initial breakdown pulses.

221 Figure 3 shows key processes seen in the HC-1 records inside the solid-line rectangular
222 box in Figure 2a after the formation of horizontal channel aloft. Four bidirectional leaders
223 (BL₁-BL₄) sequentially initiated and developed along the same predominantly vertical path
224 below the previously formed horizontal channel. The positive (lower) end of each following
225 bidirectional leader was closer to the ground than that of the preceding one (see Figures 3b, 3d,
226 3f, and 3h). The lengths of four bidirectional leaders (BL₁-BL₄) progressively increased by
227 approximately 190 m from BL₁ to BL₂, 250 m from BL₂ to BL₃, and 370 m from BL₃ to BL₄.
228 The sequence of four bidirectional leaders (BL₁-BL₄) served to form a new downward positive
229 branch of the horizontal channel. The newly formed downward branch gradually decayed
230 within ~0.3 ms (see Figures 3h and 3i) and became undetectable (see Figure 3j). Then this
231 branch reilluminated (see Figure 3k) and continued extending toward ground. Comparing the
232 positions of its tip in Figures 3h and 3k, we found that the downward branch elongated by ~160
233 m, while its luminosity was undetectable for ~0.45 ms (see Figure 3j).



234

235 **Figure 3.** Key processes seen in HC-1 (50- μ s interframe interval) records inside the solid-line
 236 rectangular box shown in Figure 2a after the formation of horizontal channel aloft: (a) first
 237 image of the first bidirectional leader (BL₁) channel, (b) composite image showing maximum
 238 extent of the BL₁ channel, (c) first image of the second bidirectional leader (BL₂) channel, (d)
 239 composite image showing maximum extent of the BL₂ channel, (e) first image of the third
 240 bidirectional leader (BL₃) channel, (f) composite image showing maximum extent of the BL₃
 241 channel, (g) first image of the fourth bidirectional leader (BL₄) channel, (h) composite image

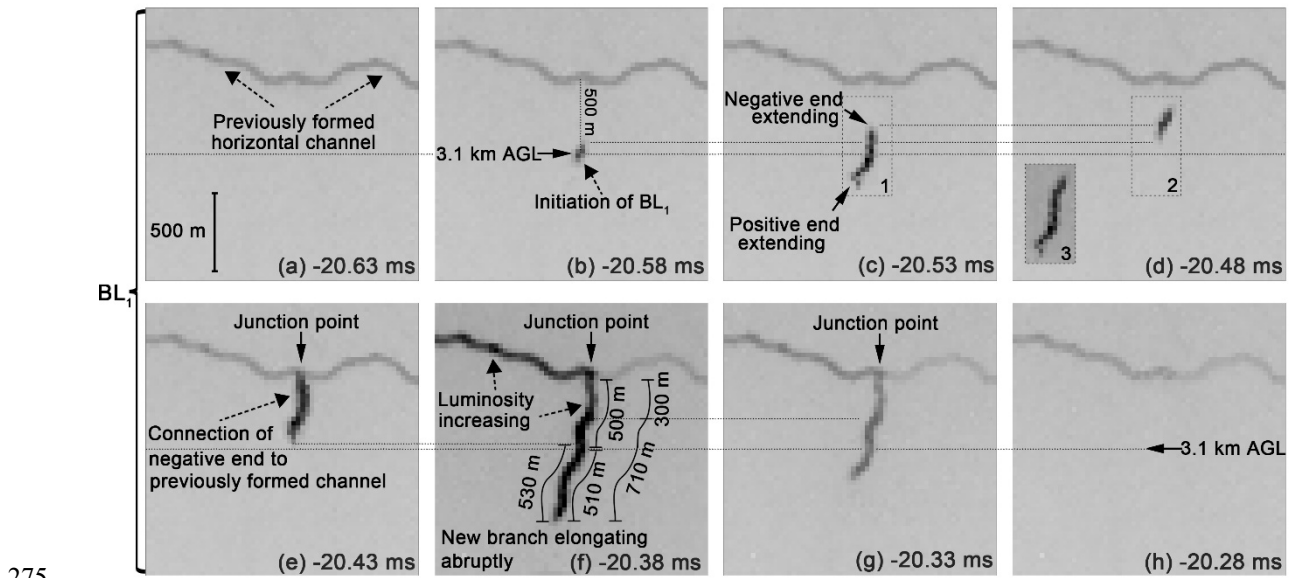
242 showing maximum extent of the BL₄ channel, (i) image of decaying fourth bidirectional leader
243 (BL₄) channel (downward branch), (j) image in which the downward branch is undetectable, (k)
244 first image showing reillumination of the downward branch formed via the sequence of BL₁ to
245 BL₄, (l) composite image showing the fully formed downward positive leader, (m) image of the
246 return-stroke early stage, (n) composite image showing the return-stroke later stage and
247 continuing current. Time labels correspond to the end of frame exposure times measured with
248 respect to the return stroke onset. Images from 0.02 to 0.92 ms are overexposed.

249 Then the re-illuminated downward branch evolved into a fully developed downward
250 positive leader (see Figure 3l), attached to the ground, and initiated a +CG return stroke (see
251 Figure 3m). Based on (not shown here) consecutive frames of HC-1 and HC-2 (obtained from
252 Movies S2 and S3 in the supporting information), the entire discharge channel (including the
253 vertical channel to ground and both left and right parts of the horizontal channel) exhibited
254 light blooming during the +CG return stroke, but the brightness increase of the left part of the
255 horizontal channel was significantly larger than that of the right part. During the later stage of
256 return stroke and continuing current, the left part maintained elevated brightness, while the
257 right part just returned to the brightness level seen before the return stroke (see Figure 3n).
258 Therefore, as noted earlier, it appears that mostly the left part was active during the positive
259 leader/return stroke sequence, although the right part also contributed some current,
260 particularly during the continuing current stage, as seen in Figure 7.

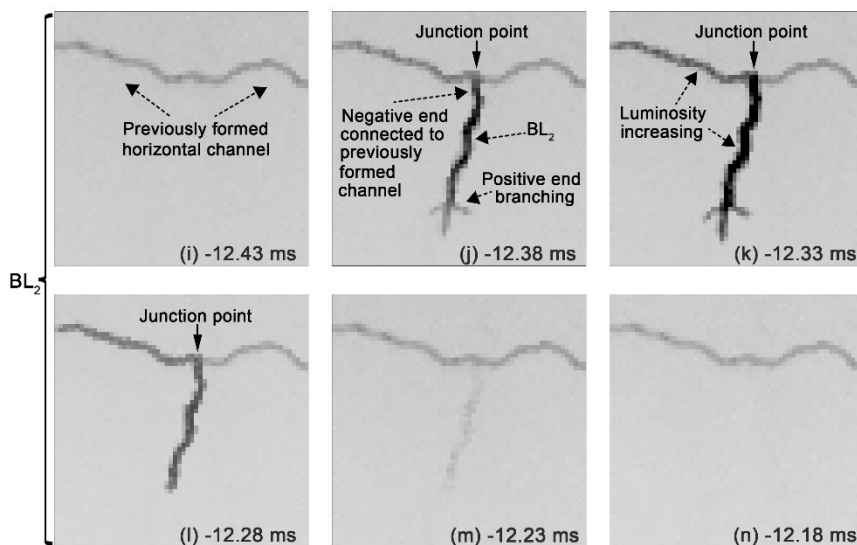
261 Figures 4a-4h show 8 consecutive images of BL₁, and 6 consecutive images of BL₂ are
262 shown in Figures 4i-4n. BL₁ initiated at a height of 3.1 km AGL and at a distance of ~500 m
263 from the horizontal channel above it. Its bidirectional extension is clearly seen in Figures 4b
264 and 4c, although its lower end became undetectable in Figure 4d. By overlaying BL₁ images
265 labeled 1 and 2 in Figures 4c and 4d, respectively, we obtained a composite image labeled 3 in
266 Figure 4d, which suggests that 1 and 2 had a common part. It is possible that the lower part of 1
267 decayed, while its upper part survived and eventually made connection to the horizontal
268 channel as seen in Figure 4e.

269 After the connection, the luminosity of BL₁ and the left part of the horizontal channel
270 increased significantly, while the luminosity of its right part diminished (see Figure 4f). The

271 connection was also associated with elongation of BL₁ channel by approximately 530 m (see
 272 Figure 4f), retracing the previously formed but decayed BL₁ channel seen in Figure 4c. The
 273 effective 2-D elongation speed was approximately 1.1×10^7 m/s. Then the new positive branch
 274 formed by BL₁ gradually decayed (see Figure 4g) and became undetectable in Figure 4h.



275



276

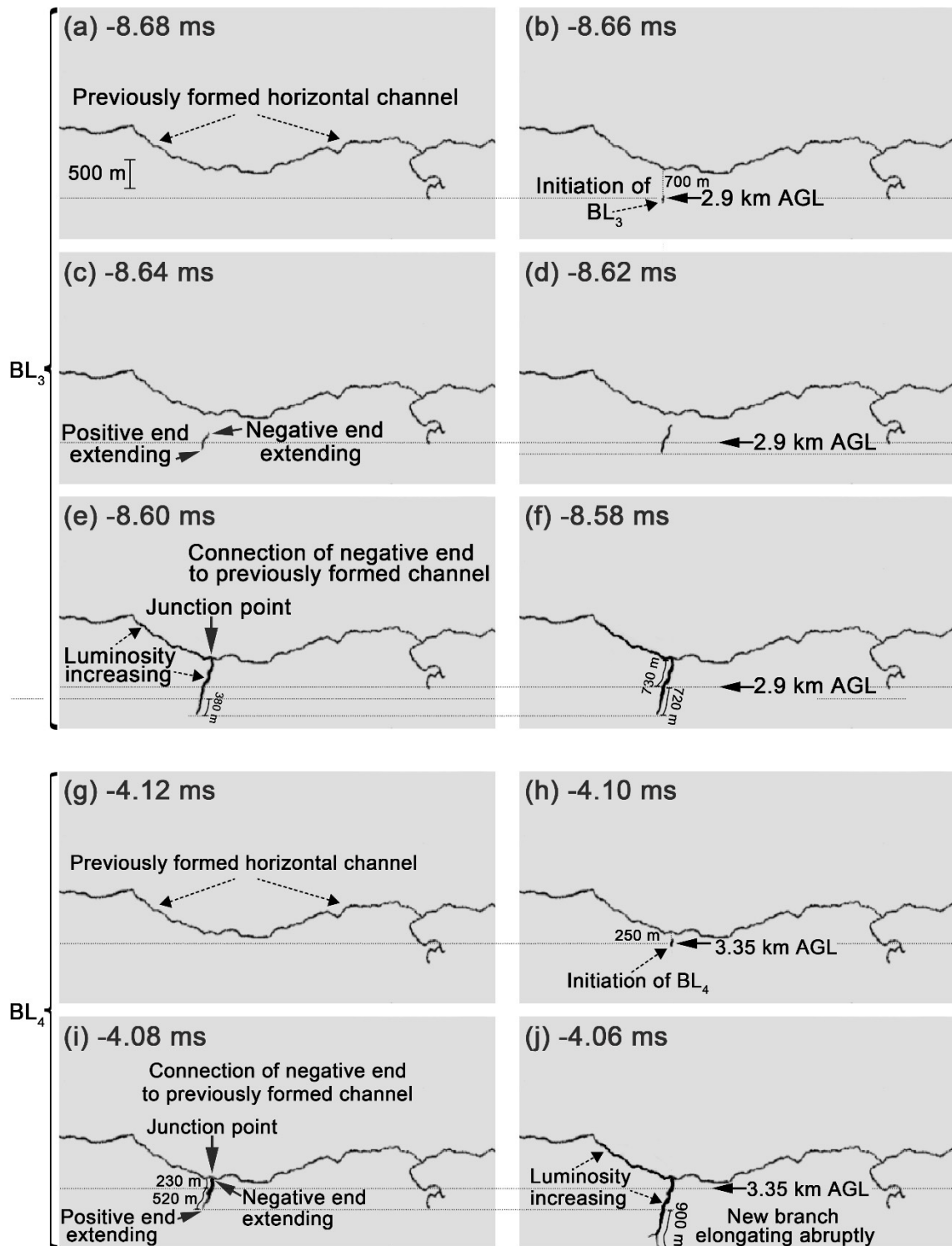
277 **Figure 4.** (a-h) Eight consecutive HC-1 (50- μ s interframe interval) images of the evolution of
 278 first bidirectional leader (BL₁) and (i-n) six consecutive HC-1 images of the second
 279 bidirectional leader (BL₂) within the small dotted-line rectangular box shown in Figure 2a. The
 280 solid-line rectangular box labeled 3 in panel (d) is a superposition of boxes labeled 1 and 2 in
 281 panels (c) and (d), respectively. Each image was inverted and contrast enhanced. The time

282 stamp given on each image is the end of the exposure time. For BL₂, no upward extension was
283 detected, probably due to insufficient time resolution of the camera or low (undetectable)
284 brightness of BL₂ channel in (i). BL = bidirectional leader; AGL = above ground level.

285 It is unknown whether the polarity reversal (neutral) point of BL₁ was stationary at 3.1
286 km AGL (see Figure 4b) or moved up as its lower part decayed (see Figure 4d). In the former
287 case, the extension of the negative end was approximately 500 m (see Figure 4f), which is
288 about the same as the extension of the positive end (approximately 510 m). In the latter case,
289 the extension of the negative end was approximately 300 m (see Figure 4f), with the positive
290 end extension being approximately 710 m.

291 Figure 4i shows the frame just preceding the occurrence of BL₂ (7.85 ms after the decay
292 of BL₁). In its first image (Figure 2j), BL₂ appears to be already connected to the horizontal
293 channel aloft, which can be due to insufficient temporal resolution of the camera or low
294 (undetectable) brightness of BL₂ channel in Figure 4i. BL₂ followed the decayed channel of
295 BL₁ (compare Figures 4j and 4f). Further, the brightness of the new branch formed by BL₂ and
296 the left part of the horizontal channel in Figure 4k increased, similar to Figure 4f. This
297 similarity makes us believe that event BL₂ was indeed a bidirectional leader. Note branching at
298 the lower (positive) end of the BL₂ channel (see Figures 4j and 4k), which is usually considered
299 as evidence of leader extension in virgin air (e.g., Tran and Rakov 2016).

300 Unlike BL₁ and BL₂, BL₃ and BL₄ were recorded, with a better time resolution (20- μ s
301 interframe interval), by HC-2 (see Movie S3 in the supporting information), within -10 to 10
302 ms time windows shown in Figure 2b. The dynamics of BL₃ and BL₄ are shown in Figure 5.
303 Figures 5a-5f show 6 consecutive images of BL₃, which occurred approximately 3.5 ms after
304 BL₂. The initiation height of BL₃ (2.9 km AGL and 700 m below the horizontal channel) was
305 approximately 200 m lower than that of BL₁. BL₃ initiated and extended bidirectionally in the
306 remnants of the decayed channel of BL₂. Similar to BL₁, brightness of the left part of the
307 horizontal channel and that of BL₃ itself increased after the connection of the negative (upper)
308 end of BL₃ to the horizontal channel (see Figures 5e and 4f). However, in contrast to BL₁, BL₃
309 was extending without interruption until its connection to the horizontal channel (see Figures
310 5c-5e).



311

312

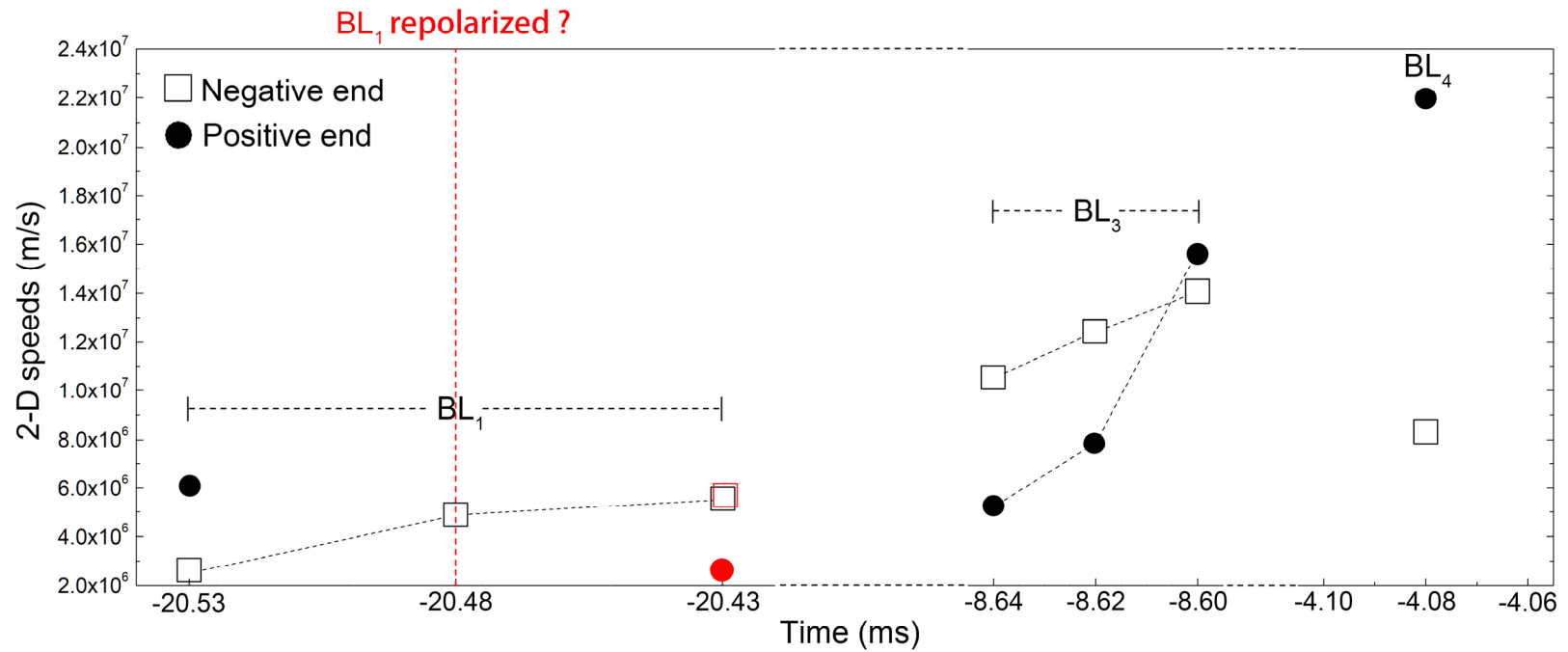
313 **Figure 5.** (a-f) Six consecutive HC-2 (20- μ s interframe interval) images of BL₃ and (g-j) four
 314 consecutive HC-2 images of BL₄. The images were background removed, inverted, and
 315 contrast enhanced. The time stamp given on each image is the end of the exposure time. The
 316 dashed-line rectangular box in Figure 2a shows the FOV of HC-2. BL = bidirectional leader;
 317 AGL = above ground level.

318 In Figure 5e, the positive (lower) end of BL₃ extended by approximately 380 m relative
319 to its position in Figure 5d. It is unknown whether this extension occurred before or after the
320 negative (upper) end of BL₃ connected to the horizontal channel aloft. No further extension is
321 seen in Figure 5f. The overall length of the negative end of BL₃ was approximately 730 m (see
322 Figure 5f), which is almost the same as that of the positive end (approximately 720 m).

323 Figures 5g-5j show 4 consecutive images of BL₄, which occurred approximately 4.5 ms
324 after BL₃. The initial height of BL₄ (3.35 km AGL and 250 m below the horizontal channel)
325 was higher than those of BL₁ and BL₃. BL₄ extended bidirectionally along the decayed channel
326 of BL₃ (see Figures 5h and 5i), and within approximately 20 μs the negative end of BL₄
327 connected to the horizontal channel (see Figure 5i). The brightness of BL₄ and the left part of
328 the horizontal channel (to the left of the junction point) increased. Due to the positive end of
329 BL₄ extending beyond the lower edge of Figure 5j, we couldn't obtain the total length of the
330 positive end of BL₄ from Figure 5j. According to Figure 3h, the overall length of BL₄ channel
331 was approximately 1820 m. The total length of the negative (upper) end of BL₄ was
332 approximately 230 m (see Figure 5i), which is considerably shorter than that of its positive
333 (lower) end (approximately 1590 m).

334 Like BL₁, BL₄ elongated abruptly (beyond the lower edge of Figure 5i) at the time of its
335 connection to the horizontal channel (see Figures 5i and 5j). The abrupt elongation was by
336 approximately 1070 m, as seen in Figure 3h, with a 2-D speed of approximately 5.4×10^7 m/s.
337 Note that, similar to BL₂, the lower (positive) end of BL₄ channel was branched (see Figure 5j),
338 which indicates that it extended into virgin air.

339 We estimated 2-D speeds of the positive and negative ends of BL₁, BL₃ and BL₄, based
340 on the consecutive frames of HC-1 and HC-2 (Figures 4a-4h, 5a-5f, and 5g-5j). Speed profiles
341 for three bidirectional leaders (BL₁, BL₃, and BL₄) are shown in Figure 6. The 2-D nonzero
342 speeds of the negative and positive ends ranged from 2.5×10^6 to 1.4×10^7 m/s and from $2.5 \times$
343 10^6 to 5.4×10^7 m/s, respectively. The average (mean) speeds of the negative and positive ends
344 were approximately 8.0×10^6 m/s and 9.9×10^6 m/s, respectively. The average (mean)
345 extension speed of BL-formed downward branches after the negative BL end connected to the
346 horizontal channel was approximately 2.5×10^7 m/s.



347

348 **Figure 6.** The 2-D speeds of negative and positive ends of the first bidirectional leader (BL₁), the third bidirectional leader (BL₃), and the
 349 fourth bidirectional leader (BL₄), based on the consecutive frames shown in Figure 4 (BL₁, HC-1) and Figure 5 (BL₃ and BL₄, HC-2).
 350 The red box and red circle represent the speeds of negative and positive ends, respectively, for the case if BL₁ was repolarized.

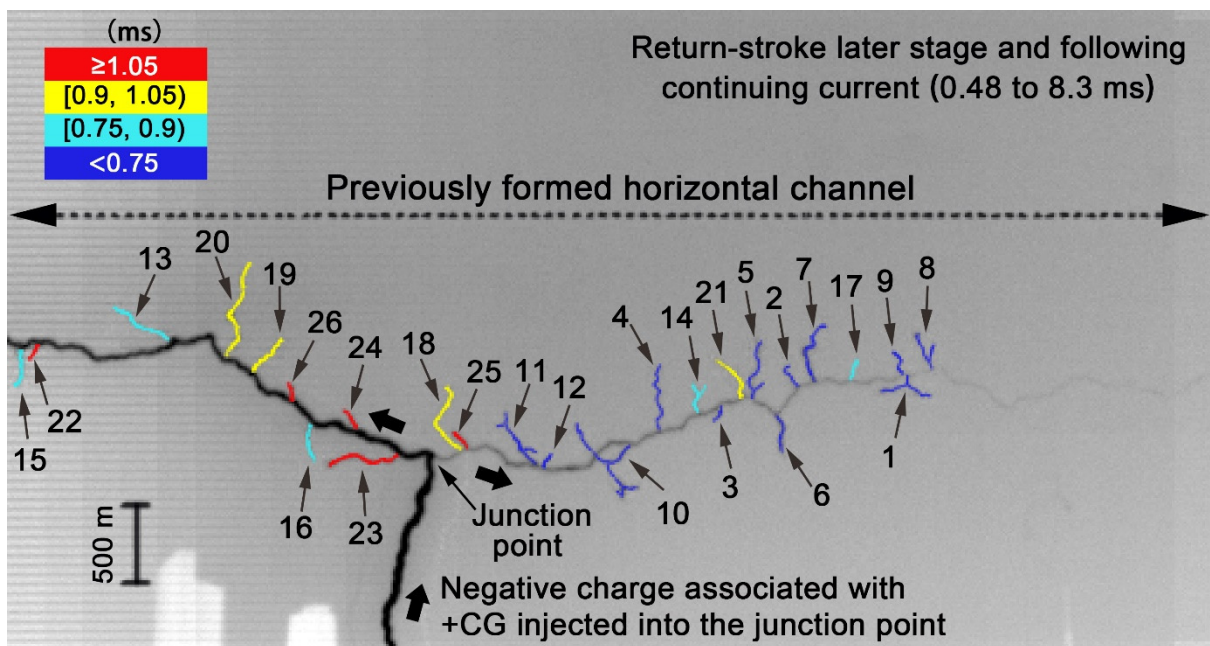
351 We now present transient streamer-like discharges from the lateral surface of the
352 horizontal channel during the return-stroke later stage and the following continuing current.
353 Figure 7 shows a composite image of 160 selected HC-2 (20- μ s interframe interval) frames for
354 the time interval of 0.48 to 8.3 ms (all after the +CG return-stroke onset). One can see 26 side
355 branches, labeled 1 through 26, extending primarily up and down (radially) from the horizontal
356 channel when the negative charge associated with the return-stroke later stage and the
357 following continuing current was injected into the horizontal channel core, probably
358 surrounded by a positive space charge sheath. These branches are numbered in the order of
359 their occurrence relative to the return stroke onset. Their time of occurrence is color coded.
360 Because these transient events were relatively far from the observation station, they produced
361 no pronounced electric field changes (see FA and SA traces in Figure 2b). These branches
362 appear to be streamer filaments originating from the lateral surface of the horizontal channel,
363 since they are fainter and thinner than their parent channel.

364 These side branches were transient; that is, they decayed soon after extending from the
365 horizontal channel. Then some of the decayed (non-luminous) side branches were
366 reilluminated by one or more recoil leader or streamer type events. At the same time, some new
367 side branches were extending from other parts of the horizontal channel. Therefore, the
368 branches seen in Figure 7 are the cumulative effect of their formation process and
369 reillumination by the recoil type processes. Note that the recoil events caused the flickering of
370 side branches.

371 Characteristics of each of the 26 streamer-like filaments, time intervals between the
372 26 side branches and their 2-D extension speeds are given in Table 1. The side (radial)
373 branches were observed within 0.48 to 2.02 ms after the onset of +CG return stroke and
374 extended away from the horizontal channel over approximately 100 to 750 m (mean = 320 m)
375 at speeds of approximately 0.5 to 1.9×10^7 m/s (mean = 1.2×10^7 m/s).

376 It is unknown whether similar streamer-like filaments occurred before 0.48 ms due to
377 overexposure of the images caused by the +CG return stroke. Before 0.75 ms, streamer-like
378 filaments appeared only on the right part of the horizontal channel. From 0.75 to 1.05 ms,
379 streamer-like filaments appeared on both the left and right parts of the horizontal channel.

380 From 1.05 to 2.20 ms, streamer-like filaments, except for #25 appeared only on the left part
 381 of the horizontal channel. No streamer-like filaments were identified between 2.02 and 8.3
 382 ms. Note that both the left and right parts of the horizontal channel increased in brightness at
 383 the return stroke onset, even though the left part was always brighter. This suggests that the
 384 entire horizontal channel contributed to supplying positive charge to the junction point (or,
 385 equivalently, the negative charge injected by +CG into the junction point moved both to the
 386 left and to the right along the horizontal channel). The hot (luminous) core of the horizontal
 387 channel was probably surrounded by a non-luminous positive space charge sheath, formed
 388 during the +CG leader stage. Negative charges pumped into the horizontal channel by the
 389 +CG return stroke and continuing current were probably the cause of side branches (negative
 390 breakdowns) developing into the positive space charge sheath.



391
 392 **Figure 7.** Composite image of 160 selected frames (from 0.48 to 8.3 ms) obtained using HC-2
 393 (20- μ s interframe interval) showing side branches (different colors indicate their occurrence
 394 relative to the RS onset) originating from the horizontal channel during the return-stroke later
 395 stage and continuing current. The composite image was inverted and contrast enhanced. Thick
 396 arrows indicate the direction of motion of negative charge associated with the +CG return
 397 stroke and continuing current along the vertical and horizontal channels. Thinner arrows
 398 (numbered 1 to 26) point to the discernible side branches (streamer-like filaments).

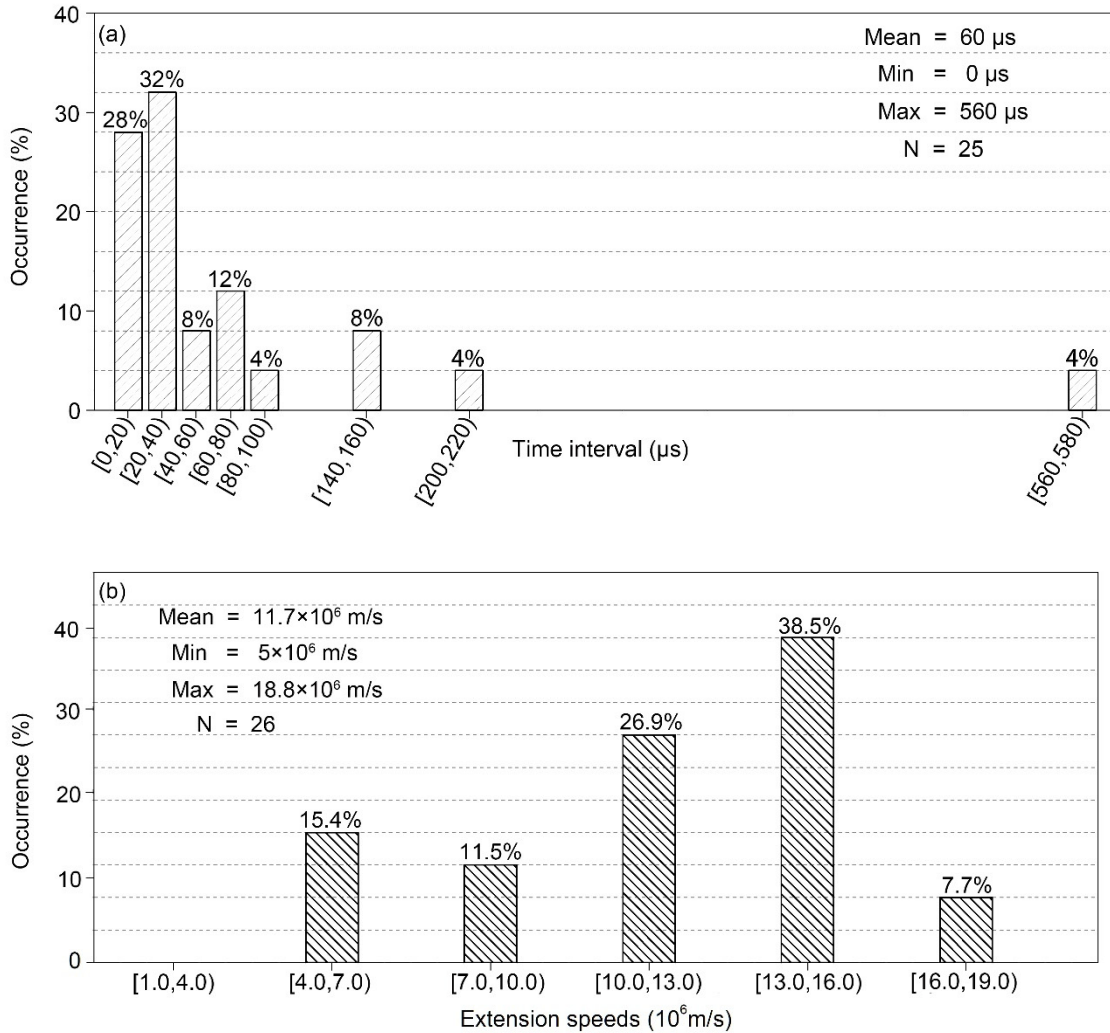
399 **Table 1.** Characteristics of 26 flickering side branches shown in Figure 7

400

Side branch ID	Initiation time relative to RS onset (ms)	2D length (m)	2D extension speeds (10^6 m/s)
1	0.48	260	13.0
2	0.52	210	10.5
3	0.52	130	6.5
4	0.54	500	12.5
5	0.54	440	11.0
6	0.56	300	15.0
7	0.6	310	15.5
8	0.6	290	14.5
9	0.62	190	9.5
10	0.64	550	13.8
11	0.7	450	11.3
12	0.7	100	5.0
13	0.78	560	14.0
14	0.78	250	12.5
15	0.84	260	13.0
16	0.86	290	14.5
17	0.88	200	10.0
18	0.9	460	11.5
19	0.9	270	13.5
20	0.92	750	18.8
21	0.98	320	16.0
22	1.18	130	6.5
23	1.74	540	13.5
24	1.88	170	8.5
25	2.02	160	8.0
26	2.02	100	5.0
Mean	0.91	320	11.7

401 Distributions of time intervals between the 26 side branches and their 2-D extension
402 speeds are shown in Figure 8. Minimum and maximum time intervals are 0 and 560 μ s,
403 respectively, with a mean value of 60 μ s. Most of the intervals (60%) are shorter than 40 μ s
404 and 84% are shorter than 100 μ s. In many cases multiple events occurred simultaneously or
405 almost simultaneously (see Table 1). The minimum and maximum extension speeds are $5 \times$

406 10^6 and 18.8×10^6 m/s, respectively, with a mean value of 11.7×10^6 m/s. The
 407 overwhelming majority (73%) of speeds are greater than 10^7 m/s.



408

409

410 **Figure 8.** (a) Distribution of time intervals between 26 side branches and (b) 2D extension speeds of
 411 26 side branches.

412 **4. Discussion and Summary**

413 A sequence of four bidirectional leaders (BL₁-BL₄) served to form a new positive
 414 branch originating from the previously formed horizontal channel aloft and eventually
 415 attached to the ground and initiated a 135-kA +CG return stroke. To the best of our
 416 knowledge, the process of formation of in-cloud channel branch that extended toward ground
 417 and caused +CG has never been documented before. Additionally, we observed (also for the

418 first time) negative streamer-like filaments extending sideways from the positively charged
419 horizontal channel in response to the injection of negative charge associated with the +CG.

420 **Initiation of vertical bidirectional leaders.** It is known (e.g., Maslowski and
421 Rakov, 2006) that the bulk of leader charge is contained in the corona (space charge) sheath
422 formed around the narrow hot core. Therefore, the horizontal channel seen in our high-speed
423 video camera images is a narrow hot core surrounded by optically undetectable corona sheath,
424 whose outer radius should be up to tens of meters (e.g., for leader line charge density of 1
425 mC/m, the corona-sheath radius should be about 20 m, according the Gauss Law). The
426 horizontal channel was positive at the time of BL₁-BL₄. The shielding effect of the positive
427 corona sheath around the positive hot core should suppress the development of branches
428 directly from the core. For this reason, such branches are more likely to be formed via
429 bidirectional leaders excited outside the positive corona sheath. BL₁ to BL₄ initiated at
430 distances of approximately 250 to 700 m from the luminous horizontal channel, from which
431 we infer that the radius of the positive corona sheath was less than 250 m. It is worth noting
432 that the radius of corona sheath for positive polarity is expected to be greater than that for
433 negative polarity (because of the lower propagation field threshold for positive streamers) and
434 that the initiation point of later BLs should be influenced by the presence of remnants of
435 preceding BLs.

436 **Dynamics of bidirectional leaders.** We start with a brief overview of the literature
437 on bidirectional leaders making connection to positively charged channels. Most of the time,
438 bidirectional leaders are completely or in part hidden inside the cloud, which makes their
439 optical imaging impossible. Therefore, as of today, there are only a few optical observations
440 of bidirectional leaders found in the literature. Montanya et al. (2015) and Warner et al. (2016)
441 reported on bidirectional leaders making connection to pre-existing positively charged
442 channels of cloud and ground lightning discharges, respectively. Further, Pilkey (2014,
443 Figures. A-1 and A-2) reported on a floating channel segment that initiated about 84 m from
444 the positive in-cloud leader channel near 3-km altitude and 364 μ s later connected to the
445 lateral surface of that channel. Tran and Rakov (2016), using a high-speed video camera,
446 observed a natural lightning discharge that started with a bidirectional leader. The negative

447 end of the bidirectional leader extended toward the ground (and eventually produced a return
448 stroke), while its positive end, developing primarily horizontally, exhibited an abrupt
449 extension that was relatively straight and had a 2-D length of about 1 km. Tran and Rakov
450 (2016) tentatively interpreted this event as a gigantic, kilometer-scale positive-leader step that
451 developed from a space stem/leader and connected to the lateral surface of the existing
452 positive channel, creating a major positive branch. This newly-created branch faded and then
453 was re-illuminated four times with a remarkably constant time interval of 1.2 ms. The rate at
454 which the new positive branch was formed was at least 1.6×10^6 m/s if it originated from the
455 mid-point of the newly-formed branch. Additionally, Pu and Cummer (2019), who used a
456 100-200 MHz broadband interferometer, observed a bidirectional leader that initiated
457 approximately 500 m from a positive in-cloud channel and whose negative end connected to
458 the positive channel.

459 In this study, the formation of new downward positive branch was facilitated by four
460 bidirectional leaders sequentially retracing the same path. The resultant downward branch
461 elongated abruptly at the time of negative end of BL₁ and BL₄ connected to the floating
462 horizontal channel (see Figures 4f and 5j). Some elongation of the positive ends of BLs prior
463 to connection could have occurred in the same frame. The lengths of abrupt elongations of
464 new branches were obtained by comparing the tip positions in the connection frame and in
465 the frame immediately after connection (see Figures 4e and 4f; Figures 5i, 5j, and 3h). The
466 abrupt extension events exhibited some similarities with the so-called restrike phenomenon
467 reported by Les Renardieres Group (1972, 1977) from long positive laboratory spark
468 experiments. However, the 2-D speeds of the abrupt extensions (BL₁, approximately 1.1×10^7
469 m/s in virgin air; BL₄, approximately 5.4×10^7 m/s along the remnants of BL₃ and extended
470 into virgin air, unless there was an optically undetectable channel prior to BL₁) were much
471 larger than the restrike speeds (0.5 to 2.0×10^5 m/s) based on the long-spark observations of
472 Chen et al. (2016). The abrupt extension lengths (approximately 510 and 1070 m) were much
473 larger than the abrupt extensions of the positive end of a dart leader (approximately 91 to 160)
474 reported by Wu et al. (2019a), but were comparable to that of the 1-km-long extension

475 occurring at the positive end of the bidirectional leader based on the observations of Tran and
476 Rakov (2016).

477 **Side branches from the lateral surface of the horizontal channel in response to**
478 **+CG.** Before the +CG return stroke, the vertical and horizontal channels each consist of a
479 narrow hot core surrounded by an optically undetectable radial corona sheath containing the
480 positive space charge deposited there by the preceding positive leader. The 135- kA +CG
481 return stroke effectively transports negative charge toward the junction point and into the
482 horizontal channel, to neutralize the positive leader charge. The negative charge (some tens
483 of coulombs expected for the 135-kA peak current) rapidly injected into the
484 horizontal-channel hot core caused negative breakdown, in the form of side branches, into the
485 positive corona sheath surrounding the hot core. The side branches extended over roughly
486 100 to 750 m (probably beyond the positive corona sheath, which is expected to have radial
487 dimension up to tens of meters) at speeds ranging from ~ 0.5 to 1.9×10^7 m/s and exhibited
488 flickering.

489 In some respects the side branches are similar to the recently discovered "needles"
490 (with no optical images reported to date). The similarities include (1) the extension from the
491 lateral surface of positively charged channels, (2) length of the order of 100 m (in our case a
492 little longer), and (3) flickering. On the other hand, extension speeds are different: 10^5 to 10^6
493 m/s for "needles" vs. of the order of 10^7 m/s for our flickering side branches. Also, "needles"
494 flicker at time intervals of some milliseconds, while in our case the time intervals are
495 considerably shorter (mean = 60 μ s; see Figure 8a). The reason for the difference in time
496 interval and speed between our streamers and their "needles" may be that the 135-
497 kA-return-stroke later stage and the following continuing current of our +CG flash injected a
498 considerably large negative charge (tens of coulombs are expected) into the positive horizontal
499 channel than charges associated with in-cloud positive leaders studied by Hare et al. (2019) and
500 Pu and Cummer (2019). Positive leader currents in upward and rocket-and-wire triggered
501 lightning are of the order of hundreds of amperes (Mike et al. 2005), more than 2 orders of
502 magnitude lower than the peak current of our +CG flash. Of course, the two phenomena
503 occur in different contexts (leader vs. return stroke), but their physics should be similar. In

504 our future work, we will quantify the characteristics of side branches in more detail and
505 compare more parameters of streamer-like filaments observed in this study and needle-like
506 structures reported by Hare et al. (2019) and Pu and Cummer (2019).

507 **Acknowledgments**

508 This work was supported in part by the National Key R&D Program of China (grant
509 2017YFC1501504), the National Natural Science Foundation of China (grant 41805005 and
510 41775010), and in part by the National Science Foundation (Grant AGS-1701484). This
511 study complies with the AGU data policy. All the lightning data supporting the conclusion of
512 the paper are available online (<https://figshare.com/s/d2131d2265e7daabe303>).

513 **References**

- 514 Chen, S., Zeng, R., Zhuang, C., Zhou, X. & Ding, Y. (2016). Experimental study on branch and
515 diffuse type of streamers in leader restrike of long air gap discharge. *Plasma Sci.*
516 *Technol.* 18, 305–310. [http://doi: 10.1088/1009-0630/18/3/15](http://doi:10.1088/1009-0630/18/3/15)
- 517 Hare, B. M., Scholten, O., Dwyer, J., Trinh, T. N. G., Buitink, S., ter Veen, S., et al. (2019).
518 Needlelike structures discovered on positively charged lightning branches. *Nature*,
519 568(7752), 360–363. <https://doi.org/10.1038/s41586-019-1086-6>
- 520 Jiang, R., Wu, Z., Qie, X., Wang, D., Liu, M. (2014). High-speed video evidence of a dart
521 leader with bidirectional development. *Geophysical Research Letters*, 41, 5246–5250.
522 <https://doi.org/10.1002/2014GL060585>
- 523 Kaneyoshi Takamatsu, Nobuyuki Takagi and Daohong Wang. (2015). Characteristics of the
524 brief but bright discharges that often occur along the trails of positive leaders. *Journal*
525 *of Atmospheric Electricity*. 35, 17-30. <https://doi.org/10.1541/jae.35.17>
- 526 Kong, X., X. Qie, and Y. Zhao (2008), Characteristics of downward leader in a positive
527 cloud-to-ground lightning flash observed by high-speed video camera and electric field
528 changes, *Geophysical Research Letters*, 35, L05816.
529 <http://doi:10.1029/2007GL032764>

530 Kostinskiy, A. Yu, V. S. Syssoev, N. A. Bogatov, E. A. Mareev, M. G. Andreev, L. M.
531 Makalsky, D. I. Sukharevsky, and V. A. Rakov (2015), Infrared images of bidirectional
532 leaders produced by the cloud of charged water droplets, *Journal of Geophysical*
533 *Research: Atmospheres*, 120, 10,728–10,735. <http://doi:10.1002/2015JD023827>

534 Les Renardieres Group (1972). Research on long air gap discharges at Les Renardieres. *Electra*
535 23, 53–157.

536 Les Renardieres Group (1977). Positive discharges in long air gaps at Les Renardieres, 1975
537 results and conclusions. *Electra* 53, 31–153.

538 Lu, W., L. Chen, Y. Zhang, Y. Ma, Y. Gao, Q. Yin, S. Chen, Z. Huang, and Y. Zhang (2012),
539 Characteristics of unconnected upward leaders initiated from tall structures observed in
540 Guangzhou, *Journal of Geophysical Research: Atmospheres*, 117, D19211.
541 <http://doi:10.1029/2012JD018035>

542 Lu, W., L. Chen, Y. Ma, V. A. Rakov, Y. Gao, Y. Zhang, Q. Yin, and Y. Zhang (2013),
543 Lightning attachment process involving connection of the downward negative leader to
544 the lateral surface of the upward connecting leader, *Geophysical Research Letters*, 40,
545 5531-5535. <http://doi:10.1002/2013GL058060>

546 Maslowski, G., & Rakov, V. A. (2006). A study of the lightning channel corona sheath. *Journal*
547 *of Geophysical Research Atmospheres*, 111(D14).
548 <https://doi.org/10.1029/2005JD006858>

549 Miki, M., V. A. Rakov, T. Shindo, G. Diendorfer, M. Mair, F. Heidler, W. Zischank, M. A.
550 Uman, R. Thottappillil, and D. Wang (2005), Initial stage in lightning initiated from tall
551 objects and in rocket-triggered lightning, *J. Geophys. Res.*, 110, D02109.
552 <https://doi:10.1029/2003JD004474>.

553 Montanyà, J., van der Velde, O., & Williams, E. R. (2015). The start of lightning: Evidence of
554 bidirectional lightning initiation. *Scientific Reports*, 5, 15180.
555 <https://doi.org/10.1038/srep15180>

556 Nag, A., & Rakov, V. A. (2012). Positive lightning: an overview, new observations, and
557 inferences. *Journal of Geophysical Research: Atmospheres*, 117(D8).
558 <https://doi.org/10.1029/2012JD017545>

559 Pilkey, J. T. (2014). The physics of lightning studied using lightning mapping array, electric
560 field, and optical measurements, PhD dissertation, University of Florida.

561 Pu Y, Cummer S A. Needles and Lightning Leader Dynamics Imaged with 100–200 MHz
562 Broadband VHF Interferometry. *Geophysical Research Letters*, 2019, 46(22). [http://doi:](http://doi:10.1029/2019gl085635)
563 [10.1029/2019gl085635](http://doi:10.1029/2019gl085635)

564 Qi, Q., Weitao, L., Bin, W., Ying, M., Luwen, C., Hengyi, L. (2018). Three-dimensional
565 optical observations of an upward lightning triggered by positive cloud-to-ground
566 lightning. *Atmospheric Research*, 214, 275-283.
567 <http://doi:10.1016/j.atmosres.2018.08.003>

568 Rakov, V. A., Uman, M. A., Rambo, K. J, Fernandez, M. I., Fisher, R. J., & Schnetzer, G. H., et
569 al. (1998). New insights into lightning processes gained from triggered-lightning
570 experiments in Florida and Alabama. *Journal of Geophysical Research*, 103(D12),
571 14117, <http://doi:10.1029/97JD02149>

572 Rakov, V. A., and M. A. Uman (2003), *Lightning: Physics and Effects*, Cambridge Univ. Press,
573 New York.

574 Saba, M. M. F., L. Z. S. Campos, E. P. Krider, and O. Pinto Jr. (2009), High-speed video
575 observations of positive ground flashes produced by intracloud lightning, *Geophysical*
576 *Research Letters*, 36, L12811. <http://doi:10.1029/2009GL038791>

577 Shao, X., C. T. Rhodes, and D. N. Holden (1999), RF radiation observations of positive
578 cloud-to-ground flashes, *Journal of Geophysical Research*, 104(D8), 9601-9608.
579 <http://doi:10.1029/1999jd900036>

580 Tran, M. D., & Rakov, V. A. (2016). Initiation and propagation of cloud-to-ground lightning
581 observed with a high-speed video camera. *Scientific Reports*, 6, 39521.
582 <http://doi:10.1038/srep39521>

583 Wang, D., Watanabe, T., & Takagi, N. (2011). A high speed optical imaging system for
584 studying lightning attachment process. 7th Asia-Pacific International Conference on
585 Lightning. <https://doi.org/10.1109/apl.2011.6111050>

586 Warner, T. A., Saba, M. M. F., Schumann, C., Helsdon, J. H. and Orville, R. E (2016).
587 Observations of bidirectional lightning leader initiation and development near positive
588 leader channels. *Journal of Geophysical Research: Atmospheres*, 121, 9251-9260.
589 [http://doi: 10.1002/2016JD025365](http://doi:10.1002/2016JD025365)

590 Wu, B., Lyu, W., Qi, Q., Ma, Y., Chen, L., Jiang, R., et al. (2019a). High-speed video
591 observations of recoil leaders producing and not producing return strokes in a Canton-
592 Tower upward flash. *Geophysical Research Letters*, 46, 8546–8553.
593 <http://doi:10.1029/2019GL083862>

594 Wu, B., Lyu, W., Qi, Q., Ma, Y., Chen, L., Zhang, Y., et al. (2019b). Synchronized two-station
595 optical and electric field observations of multiple upward lightning flashes triggered by
596 a 310 kA +CG flash. *Journal of Geophysical Research: Atmospheres*, 124, 1050–1063.
597 <https://doi.org/10.1029/2018JD02937>

598 Yuan, S., Jiang, R., Qie, X., Sun, Z., Wang, D., Zhang, Y. Zhu, Y., Rakov, V., A (2018).
599 Development of side bidirectional leader and its effect on channel branching of the
600 progressing positive leader of lightning. *Geophysical Research Letters*, 46, 1746-1753.
601 <http://doi:10.1029/2018GL080718>